Chapter 5

First principles potentials for Al-(Ti, Zr)-(Ni, Cu) system

5.1 Introduction

The prediction of materials properties using only first principles has been actively pursued in computational materials science (Goddard III, 2000). The first principle method is defined as the method that requires no empirical input and quantum mechanics (QM) is used as its foundation. QM provides the wave function, which is a solution to Schrodinger's equation. From the wave function, all physical properties can be derived. However, in most cases, the Shrodinger equation cannot be solved analytically. Notable exceptions are the free particle, harmonic oscillator, and hydrogen atom systems (Thijssen, 1999). Subsequently, many theories have been developed, such as the Hartree-Fock theory and density functional theory (DFT) (Thijssen, 1999; Koch, 2001). In particular, DFT has been shown to be relatively accurate compared to experiments in calculations of atoms and molecules (Hohenberg and Kohn, 1964; Kohn and Sham, 1965). Despite these successes, the practical applications for DFT have been limited by time and length scales of QM. To overcome this challenge, a hierarchy of methodologies has been proposed (Fig. 5-1) (Goddard III, 2000). In this paradigm, the important physical properties are derived from each step and then subsequently used to obtain effective parameters for the next step. Based on this approach, we perform first principle calculations of Al, Ti, Ni, Cu, Zr, and their alloys. The necessary physical properties are derived from QM and then used as an input to obtain the parameters for molecular dynamics (MD) simulations. Then, MD simulations are carried out to study the

thermodynamic properties of the alloys systems. In particular, the glass forming ability (GFA) is studied to aid the new metallic glass forming alloy development. Using the packing fraction as an indicator for GFA, MD results show that GFA increases around $Al_{40}Ti_{10}Ni_{50}$ and $Al_{20}Ti_{10}Ni_{70}$ composition in AlTiNi system.

5.2 Quantum mechanics calculations

First, the norm-conserving pseudopotentials are generated for Al, Ti, Ni, Cu, and Zr using the fhi98PP program (Fuchs and Scheffler, 1999) as shown in Fig. 5-2. The norm-conserving pseudopotential approach provides an effective and reliable means for performing DFT calculations (Bockstedte *et al.*, 1997). The important features of this approach are as follows.

- the core states are assumed to be chemically inert
- the potential does not diverge in the core region
- the wavefunction satisfies the norm-conservation condition

Subsequently, the Gaussian basis sets for the norm-conserving pseudopotentials are developed. Mathematically and numerically, the Gaussian basis formalism is one of the most efficient to implement for DFT calculations (Schultz, 2000). Using the pseudopotentials and Gaussian basis sets as inputs, the QM calculations are carried out using SeqQuest program (Schultz, 2000). The theoretical basis of SeqQuest is DFT with the local density approximation (LDA) or generalized gradient approximation (GGA). LDA assumes the constant electron gas density, which is a fairly good approximation for simple metals such as sodium. GGA accounts the non-homogeneity of the true electron density by including the gradients of the charge density in calculations. LDA is known to

underestimate bond lengths or lattice parameters in crystals, while GGA overcorrects the shortcomings of LDA (Thijssen, 1999). In this thesis, we have used GGA to calculate the properties of simple metal and transition metals in the framework of DFT.

The energy as a function of atomic volume of the system is obtained using QM. The obtained relationship between energy and volume is called the equation of state (EOS). We have calculated the EOS of 6 different crystalline phases for Al, Ti, Ni, Cu, Zr: FCC, HCP, BCC, A15, simple cubic (SC), and diamond (DM). The result for Al is shown in Fig. 5-3 and the equilibrium data of each phase are summarized in Table 5-1(a). The equilibrium properties are derived from the QM results using a universal energy function (Rose *et al.*, 1984). The EOS and equilibrium properties for Ti (Fig. 5-4 and Table 5-2(a)), Ni (Fig. 5-5 and Table 5-3(a)), Cu (Fig. 5-6 and Table 5-4(a)), and Zr (Fig. 5-7 and Table 5-5(a)) are shown in the same manner. The QM results and experimental data show good agreement (Table 5-6).

The EOS of alloy phases, such as Al_xTi_{1-x}, Al_xNi_{1-x}, and Ti_xNi_{1-x}, are also obtained. The alloys structures employed in this study are $AuCu_3$ for x=0.25 and x=0.75. For x=0.50, CsCl and NaCl structures are used. The EOS and equilibrium data for Al_xTi_{1-x}, Al_xNi_{1-x}, and Ti_xNi_{1-x} are shown in Fig. 5-8, Table 5-7(a), Fig. 5-9, Table 5-8(a), Fig. 5-10, and Table 5-9(a), respectively. The QM calculations of alloy phases show good agreement with the available experimental data, such as the lattice constant and the heat of formation (ΔH) (Hultgren, 1973; Villars, 1991).

5.3 The force-field parameters for pure metals

As introduced in Chapter 1, the Sutton-Chen potential describes the energy U of atom i as (Sutton and Chen, 1990)

$$U_i = \frac{1}{2}\sum_{j\neq i}^{N} e_{ij}\left(\frac{a_{ij}}{r_{ij}}\right)^n - c_i e_{ii}\sqrt{\sum_{j\neq i}^{N}\left(\frac{a_{ij}}{r_{ij}}\right)^m} \quad . \tag{5-1}$$

In a pure system, the Eq. 5-1 can be simplified as

$$U_i = \frac{1}{2}\sum_{j\neq i}^{N} e\left(\frac{a}{r_{ij}}\right)^n - ce\sqrt{\sum_{j\neq i}^{N}\left(\frac{a}{r_{ij}}\right)^m} \quad . \tag{5-2}$$

Here, r_{ij} is the distance between atom i and j. e sets the overall energy scale, c is a dimensionless parameter scaling the attractive term and a is a length parameter.

Since Eq. 5-2 contains a lattice sum such as $S_n = \sum_{j\neq i}^{N}\left(\frac{a}{r_{ij}}\right)^n$, it is convenient to introduce quantities d_{ij} such that $r_{ij} = a_0 d_{ij}$, where a_0 is the lattice constant of an FCC crystal. In this work, we restrict the lattice sums to $r_{ij}=2a_0$ so that we can include up to the 8th nearest neighbors (N=140) interactions of an FCC crystal in calculating the potential function. Thus, $d_{ij}=\frac{\sqrt{2}}{2}$, 1, $\frac{\sqrt{6}}{2}$, $\sqrt{2}$, $\sqrt{2.5}$, $\sqrt{3}$, $\frac{\sqrt{14}}{2}$, 2.

Using d_{ij}, S_n can be written as

$$S_n = \sum_{j\neq i}^{N}\left(\frac{a}{r_{ij}}\right)^n = \sum_{j\neq i}^{N}\left(\frac{a}{a_0 d_{ij}}\right)^n = \left(\frac{a}{a_0}\right)^n \sum_{j\neq i}^{N}\left(\frac{1}{d_{ij}}\right)^n \quad . \tag{5-3}$$

If we set a equal to a_0, S_n is simplified to

$$S_n = \sum_{j\neq i}^{N}\left(\frac{1}{d_{ij}}\right)^n \quad . \tag{5-4}$$

Then the Eq. 5-2 can be rewritten as

$$U_i = \frac{e}{2} S_n - ce\sqrt{S_m} \,. \tag{5-5}$$

Since parameter a is determined as a_0 for the convenience of the lattice sum, other force field parameters such as e, c, m, and n in Eq. 5-5 should be determined subsequently to satisfy the material properties that we are interested in. To do so, let's first consider three fundamental equilibrium material properties such as cohesive energy E_{coh}, atomic volume Ω, and bulk modulus B, which are expressed as following equations

$$U_i\big|_{r=a_0} = -E_{coh} = \frac{e}{2} S_n - ce\sqrt{S_m} \,, \tag{5-5}$$

$$\begin{aligned} P &= -\frac{\partial U_i}{\partial \Omega} = -\frac{N_{atom}}{3}\frac{1}{a_0^2}\frac{\partial U_i}{\partial r}\bigg|_{r=a_0} \\ &= -\frac{N_{atom}}{3}\frac{1}{a_0^2}\left(-\frac{e}{2}\frac{1}{a_0} n S_n + ce\frac{1}{a_0}\frac{m}{2}\sqrt{S_m}\right) = 0 \end{aligned} \,, \tag{5-6}$$

$$\begin{aligned} B &= \Omega\frac{\partial U_i}{\partial \Omega^2} = \frac{N_{atom}}{9}\frac{1}{a_0}\frac{\partial^2 E_i}{\partial r^2}\bigg|_{r=a_0} \\ &= \frac{N_{atom}}{9}\frac{1}{a_0}\left\{\frac{e}{2}\frac{1}{a_0^2} n(n+1) S_n - ce\frac{1}{a_0^2}\frac{m}{2}\left(\frac{m}{2}+1\right)\sqrt{S_m}\right\} \end{aligned} \,. \tag{5-7}$$

Here, P is pressure and N_{atom} is an integer number such that $\Omega = \frac{a_0^3}{N_{atom}}$. Then, the Eq. 5-5~5-7 can be simplified to

$$c = \frac{n S_n}{m\sqrt{S_m}}, \tag{5-8}$$

$$e = \left(\frac{2m}{2n-m}\right)\frac{E_{coh}}{S_n}, \tag{5-9}$$

$$nm = \frac{18B\Omega}{E_{coh}}. \qquad (5\text{-}10)$$

Therefore, if we choose e, c, m, and n that satisfies Eq. 5-8~5-10, the potential function Eq. 5-2 automatically reproduces given E_{coh}, Ω, and B accurately. However, we have only 3 equations for 4 parameters so far. Thus, we need additional material properties to determine the FF parameters.

Previously, Sutton and Chen used elastic constants C_{ij} of materials as additional material properties to choose the best FF parameter set (Sutton and Chen, 1990). First, they reduced the number of FF parameter candidate sets by restricting n and m only to integer numbers that closely satisfy Eq. 5-10. As a result, the potential function fails to describe B exactly. Then, e, c are determined using Eq. 5-8 and 5-9. Using the obtained FF parameter sets, C_{ij} are calculated and compared to the experimental values. The best FF parameter set is chosen as the one that gives the closest agreement with the experimental C_{ij} values.

Instead of using C_{ij}, we use the EOS data obtained from QM to determine the best FF parameter set. The procedure is as follows. First, a is set to the lattice constant of FCC phase obtained from QM. Then E_{coh_FCC}, Ω_{FCC}, and B_{FCC}, which are also obtained from QM, are used to define relationships among e, c, m, and n (Eq. 5-8~5-10). Here, we allow non-integer m and n to have more accurate description of B. Finally, to determine the best FF parameter set, we use the following QM results.

- The energy-volume curve of FCC phase
- The pressure-volume curve of FCC phase
- The E_{coh} of HCP, BCC, A15, SC, DM phases

- The *W* of HCP, BCC, A15, SC, DM phases

This is accomplished by using the cost function:

$$C = \sum_{V_i} \left|\Delta U_{FCC}^{FF}(V_i)\right| w_i^U + \sum_{V_i} \left|\Delta P_{FCC}^{FF}(V_i)\right| w_i^P + \sum_{k=1}^{5} \left|\Delta U_k^{FF}\right| w_k^U + \sum_{k=1}^{5} \left|\Delta P_k^{FF}\right| w_k^P , \qquad (5\text{-}11)$$

where $DU_{FCC}^{FF}(V_i)=U_{FCC}^{FF}(V_i)-U_{FCC}^{FF}(W_{FCC})=U_{FCC}^{FF}(V_i)+E_{coh\_FCC,}$

$DP_{FCC}^{FF}(V_i)=P_{FCC}^{FF}(V_i)-P_{FCC}^{FF}(W_{FCC})= P_{FCC}^{FF}(V_i),$

$DU_k^{FF}=U_k^{FF}(W_k)-U_{FCC}^{FF}(W_{FCC})= U_k^{FF}(W_k)+E_{coh\_FCC},$

$DP_k^{FF}=P_k^{FF}(W_k)-P_{FCC}^{FF}(W_{FCC})= P_k^{FF}(W_k),$

$w_i^P = 1/(\left|\Delta U_{FCC}^{QM}(V_i)\right|, w_i^U = 100 w_i^P ,$

$w_k^P = 1/\left|\Delta U_k^{QM}\right|, \; w_k^U = 100 w_k^P ,$

$0.83843W \pounds V_i \pounds W$ and $k=HCP, BCC, A15, SC, DM.$

The superscript FF means the results obtained from FF and QM means the results obtained from QM. The each term in Eq. 5-11 represents the contributions from QM results, which are described above in order, in the optimization process of FF parameters. w_i^P , w_i^U , w_k^P , and w_k^U are weighting functions in the cost function, which are inversely proportional to the energy difference with the stable FCC phase. In this way, we give more importance to the low energy phase. Also we set the weighting function ratio between *U* and *P* as 100, because the *U* and *P* scales about O(10^2) in units that we use in this study (Fig. 5-3~5-7).

Following the procedure described above, force field parameters are optimized to fit the SC potential based on QM results. The obtained force field parameters are shown in Table 5-1(b)~5-5(b) for Al, Ti, Ni, Cu, and Zr, respectively. The comparisons between the FF results and the QM results for each phases are shown in Table 5-1(c)~5-5(c). As

we expect, the FF describes the lower energy phases more accurately than the higher energy phases.

5.4 The force-field parameters for alloys

In a binary A-B alloy system, there are A-A, B-B and A-B interactions. A-A and B-B interactions can be described by using the force-field parameters obtained from pure A system and pure B system. To accurately describe an A-B interaction, the force field parameter set (a_{AB}, e_{AB}, c_{AB}, m_{AB} and n_{AB}) for A-B interaction is also needed. Previously, this was determined by the following expressions, which is called the mixing rule (Rafiitabar and Sutton, 1991):

$$a_{AB} = \sqrt{a_{AA} a_{BB}}\,, \tag{5-12}$$

$$e_{AB} = \sqrt{e_{AA} e_{BB}}\,, \tag{5-13}$$

$$m_{AB} = \frac{(m_{AA} + m_{BB})}{2}, \tag{5-14}$$

$$n_{AB} = \frac{(n_{AA} + n_{BB})}{2}, \tag{5-15}$$

where a_{AA}, e_{AA}, m_{AA} and n_{AA} are respectively a, ε, m and n of the pure A system. Similarly, a_{BB}, e_{BB}, m_{BB} and n_{BB} are a, ε, m and n of the pure B system. Note that there is no mixing rule for c because c is assumed to be dependent only on the type of the atom at which the local energy is evaluated (Sutton and Chen, 1990).

To accurately describe the A-B interaction, we allow that c and e in the second term of Eq. 5-1 depends also on the type of interaction. Then, the modified the SC potential for alloy system can be obtained as:

$$U_i = \frac{1}{2}\sum_{j\neq i}^{N} e_{ij}\left(\frac{a_{ij}}{r_{ij}}\right)^{n} - \sqrt{\sum_{j\neq i}^{N} c_{ij}^2 e_{ij}^2 \left(\frac{a_{ij}}{r_{ij}}\right)^{m}} \tag{5-16}$$

Consider now A_xB_{1-x} binary alloy system. The energy of atom A in site *i* is written as:

$$U_A = \frac{e_{AA}}{2}\left(\frac{a_{AA}}{L}\right)^{n_{AA}}\sum_{j\neq i}^{N} d_{Aj}\left(\frac{1}{d_{ij}}\right)^{n_{AA}} + \frac{e_{AB}}{2}\left(\frac{a_{AB}}{L}\right)^{n_{AB}}\sum_{j\neq i}^{N}(1-d_{Aj})\left(\frac{1}{d_{ij}}\right)^{n_{AB}} - \sqrt{e_{AA}^2 c_{AA}^2\left(\frac{a_{AA}}{L}\right)^{m_{AA}}\sum_{j\neq i}^{N} d_{Aj}\left(\frac{1}{d_{ij}}\right)^{m_{AA}} + e_{AB}^2 c_{AB}^2\left(\frac{a_{AB}}{L}\right)^{m_{AB}}\sum_{j\neq i}^{N}(1-d_{Aj})\left(\frac{1}{d_{ij}}\right)^{m_{AB}}}, \tag{5-17}$$

and the energy of atom B in site *i* is written as:

$$U_B = \frac{e_{BB}}{2}\left(\frac{a_{BB}}{L}\right)^{n_{BB}}\sum_{j\neq i}^{N}(1-d_{Aj})\left(\frac{1}{d_{ij}}\right)^{n_{BB}} + \frac{e_{AB}}{2}\left(\frac{a_{AB}}{L}\right)^{n_{AB}}\sum_{j\neq i}^{N} d_{Aj}\left(\frac{1}{d_{ij}}\right)^{n_{AB}} - \sqrt{e_{BB}^2 c_{BB}^2\left(\frac{a_{BB}}{L}\right)^{m_{BB}}\sum_{j\neq i}^{N}(1-d_{Aj})\left(\frac{1}{d_{ij}}\right)^{m_{BB}} + e_{AB}^2 c_{AB}^2\left(\frac{a_{AB}}{L}\right)^{m_{AB}}\sum_{j\neq i}^{N} d_{Aj}\left(\frac{1}{d_{ij}}\right)^{m_{AB}}}, \tag{5-18}$$

where d_{Aj} is 1 if site *j* is occupied by an A atom or else 0. Then, the total atomic energy of the A_xB_{1-x} binary alloy system is

$$U = xU_A + (1-x)U_B \tag{5-19}$$

Subsequently, the pressure of the A_xB_{1-x} binary alloy system is

$$P = -\frac{N_{atom}}{3}\frac{1}{a_{AB}^2}\frac{\partial U}{\partial a}\bigg|_{a=a_{AB}} = -\frac{N_{atom}}{3}\frac{1}{a_{AB}^2}\left(x\frac{\partial U_A}{\partial a} + (1-x)\frac{\partial U_B}{\partial a}\right)_{a=a_{AB}} \tag{5-20}$$

Here, a_{AB} is the lattice constant of the A_xB_{1-x} unit cell.

Using the QM calculation results for alloy phases (Table 5-7(a)~5-9(a) and Fig. 5-8~5-10) and the Eq. 5-19~5-20, the FF parameters for A-B interactions are obtained. The procedure is as follows. First, the cost function is defined as:

$$C = \sum_k 100\left|U_k^{FF} - U_k^{QM}\right| + \sum_k \left|P_k^{FF} - P_k^{QM}\right|, \qquad (5\text{-}21)$$

where k=A_3B_1($AuCu_3$ structure), AB(NaCl structure), AB(CsCl structure), AB_3($AuCu_3$ structure). Then, the FF parameter set that minimizes the cost function is found. In this optimization process, the mixing rule is used as an initial guess. Since there is no mixing rule for c_{AB}, we use $c_{AB} = \sqrt{c_{AA}c_{BB}}$ as an initial guess. The next FF parameter set is defined by changing the previous FF parameters by $-d$, 0, and $+d$. Ideally, d should be chosen considering the overall scale of each parameter. However, we use the uniform d=10^{-5} for all FF parameters in this work. By changing each FF parameters by $-d$, 0, and $+d$, 3^5 FF parameter sets are generated. Among these, the FF parameter set that minimizes the cost function is selected for the next step. This procedure continues until the FF parameter set converges. The obtained parameters are summarized in Table 5-7(b)~5-9(b). The comparisons are made between the force field results and the QM results, shown in Table 5-7(c)~5-9(c).

5.5 The extension to ternary systems

Using the developed FF parameter set (Table 5-1(b)~5-3(b) and 5-7(b)~5-9(b)), the MD simulations are done on binary, ternary, and higher order systems. The direct comparison between the QM calculations and the force-field results should be made to validate this extension to higher order systems.

In this work, the system of interest is the Al-Ti-Ni ternary system. The aluminum based intermetallics, such as Al-Ti and Al-Ni, are known to have high strength, high thermal stability, and high oxidation resistance. Therefore, our objective is to understand

and predict the phase behavior of Al-Ti-Ni system to guide the better alloy development, particularly, metallic glasses.

Starting from the random FCC solid solution, we have melted and quenched the $Al_xTi_yNi_{(1-x-y)}$ samples using *TtN* dynamics (Ray and Rahman, 1984, 1985). Due to the fast cooling rate (4×10^{12} K/s), glasses are formed in a very broad regime of the ternary phase diagram. As the initial estimation of the glass forming ability, we have used the packing efficiency as our indicator. The packing efficiency is defined as:

$$f = \frac{V_{atom}}{V_{total}} \tag{5-22}$$

Here, V_{atom} is the volume of atoms in the system and V_{total} is the total volume of the system. For example, FCC system with hard sphere approximation gives f~0.74 and f can increase if the soft sphere approximation is used (Haile, 1997). Also, f is related to the free volume of the system by

$$V_{free} = V_{total}(1-f), \tag{5-23}$$

thus, f can be used in connection with the free volume theory (Cohen and Grest, 1979, 1981) to estimate the glass transition behavior. Or intuitively, if the nature of system is similar, the less free volume results the high viscosity. Therefore, the system with less free volume have higher barrier for crystal nucleation, thus, can achieve higher degrees of supercooling, which increases the GFA.

The calculated packing efficiency in the series of $Al_xTi_yNi_{(1-x-y)}$ system during the quenching process is shown in Fig. 5-11. The packing efficiency changes smoothly as a function of concentrations. We predict that the region with the high packing efficiency

such $Al_{40}Ti_{10}Ni_{50}$ and $Al_{20}Ti_{10}Ni_{70}$ as will show a good glass forming ability, however the comparable experimental results are not available yet.

5.6 Conclusions

The purpose of this work is to extend the first principle calculations to metallic alloy system, with an emphasis on obtaining first-principle-based inter-atomic potentials. We perform accurate QM calculations in the framework of DFT with GGA to develop FF parameters. Then, the developed FF parameters are employed in MD calculations to study the thermodynamic properties of AlTiNi metallic alloy system. In particular, the study is focused on predicting the glass forming ability (GFA) to aid the new metallic glass forming alloy development. Using the packing fraction as an indicator for GFA, we predict that GFA increases near $Al_{40}Ti_{10}Ni_{50}$ and $Al_{20}Ti_{10}Ni_{70}$ composition in AlTiNi system.

References

Bockstedte, M., Kley, A., Neugebauer, J., and Scheffler, M. (1997). Density-functional theory calculations for poly-atomic systems: electronic structure, static and elastic properties and ab initio molecular dynamics. Comput. Phys. Commun. *107*, 187-222.

Cohen, M.H., and Grest, G.S. (1979). Liquid-Glass Transition, a Free-Volume Approach. Physical Review B *20*, 1077-1098.

Cohen, M.H., and Grest, G.S. (1981). A New Free-Volume Theory of the Glass-Transition. Annals of the New York Academy of Sciences *371*, 199-209.

Fuchs, M., and Scheffler, M. (1999). Ab initio pseudopotentials for electronic structure calculations of poly-atomic systems using density-functional theory. Comput. Phys. Commun. *119*, 67-98.

Goddard III, W.A. (2000). Materials and process simulation center (MSC).

Goddard, W.A. (2000). Materials and process simulation center (MSC).

Haile, J.M. (1997). Molecular dynamics simulation. A Wiley-Interscience Publication.

Hohenberg, P., and Kohn, W. (1964). Inhomogeneous Electron Gas. Phys. Rev. B *136*, B864-&.

Hultgren, R., Desai, P. D., Hawkins, D. T., Gleiser, M., Kelly, K. K. (1973). Selected values of the thermodynamic properties of binary alloys. American society for metals.

Koch, W.a.H., M. C. (2001). A chemist's guide to density functional theory. Wiley-VCH.

Kohn, W., and Sham, L.J. (1965). Self-Consistent Equations Including Exchange and Correlation Effects. Physical Review *140*, 1133-&.

Rafiitabar, H., and Sutton, A.P. (1991). Long-Range Finnis-Sinclair Potentials for Fcc Metallic Alloys. Philosophical Magazine Letters *63*, 217-224.

Ray, J.R., and Rahman, A. (1984). Statistical Ensembles and Molecular-Dynamics Studies of Anisotropic Solids. Journal of Chemical Physics *80*, 4423-4428.

Ray, J.R., and Rahman, A. (1985). Statistical Ensembles and Molecular-Dynamics Studies of Anisotropic Solids .2. Journal of Chemical Physics *82*, 4243-4247.

Rose, J.H., Smith, J.R., Guinea, F., and Ferrante, J. (1984). Universal Features of the Equation of State of Metals. Phys. Rev. B *29*, 2963-2969.

Schultz, P.A. (2000). GaN tutorial for SeqQuest: Bulk systems, Hexagonal GaN.

Sutton, A.P., and Chen, J. (1990). Long-Range Finnis Sinclair Potentials. Philos. Mag. Lett. *61*, 139-146.

Thijssen, J.M. (1999). Computational Physics. Cambridge university press.

Villars, P., Calvert, L. D. (1991). Pearson's handbook of crystallographic data for intermetallic phases. ASTM International.

Table 5-1(a). The physical properties obtained from QM calculations of Al.

Structure	E_{coh} [eV/atom]	Ω [Å^3/atom]	B [GPa]
FCC	3.39	16.609	75.1
HCP	3.38	16.923	63.5
BCC	3.30	17.215	71.7
A15	3.29	17.069	73.6
SC	2.95	19.951	61.2
DM	2.40	26.024	44.1

Table 5-1(b). The Sutton-Chen force-field parameters of Al.

	a [Å]	e [meV]	c	m	n
Al	4.05009	0.23053	204.11519	3.70326	11.16800

Table 5-1(c). Comparison between Sutton-Chen force-field and QM results of Al.

Phase	*E_ff* [eV/atom]	*E_qm* [eV/atom]	*DE* [%]	Ω_*ff* [Å^3]	Ω_*qm* [Å^3]	ΔΩ [%]
FCC	-3.39	-3.39	0.00	16.609	16.609	0.000
HCP	-3.38	-3.38	0.00	16.628	16.923	1.743
BCC	-3.35	-3.30	1.52	16.853	17.215	2.103
A15	-3.30	-3.29	0.30	17.398	17.069	1.927
SC	-2.95	-2.95	0.00	20.393	19.951	2.215
DM	-2.47	-2.40	2.92	29.297	26.024	12.577

Table 5-2(a). The physical properties obtained from QM calculations of Ti.

Structure	E_{coh} [eV/atom]	Ω [Å^3/atom]	B [GPa]
FCC	4.79	17.580	105.7
HCP	4.85	17.481	113.0
BCC	4.73	17.337	100.9
A15	4.64	17.434	100.4
SC	3.94	18.523	76.4
DM	2.31	23.511	34.6

Table 5-2(b). Sutton-Chen force-field parameters of Ti.

	a [Å]	e [meV]	c	m	n
Ti	4.12758	0.86607	79.61690	4.54777	9.58993

Table 5-2(c). Comparison between Sutton-Chen force-field and QM results of Ti.

Phase	*E_ff* [eV/atom]	*E_qm* [eV/atom]	*DE* [%]	Ω_*ff* [Å^3]	Ω_*qm* [Å^3]	ΔΩ [%]
FCC	-4.79	-4.79	0.00	17.580	17.580	0.000
HCP	-4.77	-4.85	1.65	17.606	17.481	0.715
BCC	-4.74	-4.73	0.21	17.778	17.337	2.544
A15	-4.31	-4.64	7.11	18.253	17.434	4.698
SC	-4.31	-3.94	9.39	21.009	18.523	13.421
DM	-3.60	-2.31	55.844	29.694	23.511	26.298

Table 5-3(a). The physical properties obtained from QM calculations of Ni.

Structure	E_{coh} [eV/atom]	Ω [Å^3/atom]	B [GPa]
FCC	4.44	11.773	197.1
HCP	4.41	11.648	197.8
BCC	4.40	11.853	194.3
A15	4.32	12.070	183.4
SC	3.79	13.669	146.5
DM	3.13	17.973	93.8

Table 5-3(b). Sutton-Chen force-field parameters of Ni.

	a [Å]	e [meV]	c	m	n
Ni	3.61118	0.54417	109.60592	5.38318	10.90573

Table 5-3(c). Comparison between Sutton-Chen force-field and QM results of Ni.

Phase	*E_ff* [eV/atom]	*E_qm* [eV/atom]	*DE* [%]	Ω*_ff* [Å^3]	Ω*_qm* [Å^3]	ΔΩ [%]
FCC	-4.44	-4.44	0.00	11.773	11.773	0.000
HCP	-4.43	-4.41	0.45	11.791	11.648	1.228
BCC	-4.39	-4.40	0.23	11.943	11.853	0.759
A15	-4.29	-4.32	0.69	12.336	12.070	2.204
SC	-3.92	-3.79	3.43	14.363	13.669	5.077
DM	-3.25	-3.13	3.83	20.640	17.973	14.839

Table 5-4(a). The physical properties obtained from QM calculations of Cu.

Structure	E_{coh} [eV/atom]	Ω [Å^3/atom]	B [GPa]
FCC	3.49	12.939	132.6
HCP	3.44	13.259	124.6
BCC	3.48	13.012	131.1
A15	3.38	13.324	117.9
SC	3.03	14.999	99.2
DM	2.45	20.836	48.9

Table 5-4(b). Sutton-Chen force-field parameters of Cu.

	a [Å]	e [meV]	C	m	n
Cu	3.72669	0.53580	89.23846	5.31863	10.38524

Table 5-4(c). Comparison between Sutton-Chen force-field and QM results of Cu.

Phase	*E_ff* [eV/atom]	*E_qm* [eV/atom]	*DE* [%]	Ω_*ff* [Å^3]	Ω_*qm* [Å^3]	ΔΩ [%]
FCC	-3.49	-3.49	0.00	12.939	12.939	0.000
HCP	-3.49	-3.44	1.45	12.949	13.259	2.338
BCC	-3.45	-3.48	0.86	13.110	13.012	0.753
A15	-3.39	-3.38	0.30	13.511	13.324	1.403
SC	-3.10	-3.03	2.31	15.665	14.999	4.440
DM	-2.59	-2.45	5.71	22.370	20.836	7.362

Table 5-5(a). The physical properties obtained from QM calculations of Zr.

Structure	E_{coh} [eV/atom]	Ω [Å^3/atom]	B [GPa]
FCC	6.21	23.563	91.6
HCP	6.25	23.220	91.1
BCC	6.17	23.297	86.9
A15	6.10	23.334	86.7
SC	5.29	24.654	69.8
DM	3.56	32.008	32.7

Table 5-5(b). Sutton-Chen force-field parameters of Zr.

	a [Å]	e [meV]	C	m	n
Zr	4.53680	1.27078	71.67903	4.17771	9.09421

Table 5-5(c). Comparison between Sutton-Chen force-field and QM results of Zr.

Phase	E_ff [eV/atom]	E_qm [eV/atom]	DE [%]	Ω$_ff$ [Å^3]	Ω$_qm$ [Å^3]	ΔΩ [%]
FCC	-6.21	-6.21	0.00	23.563	23.563	0.000
HCP	-6.19	-6.25	0.96	23.364	23.220	0.620
BCC	-6.16	-6.17	0.16	23.581	23.297	1.219
A15	-6.08	-6.10	0.33	24.157	23.334	3.527
SC	-5.63	-5.29	6.43	27.654	24.654	12.168
DM	-4.73	-3.56	32.87	38.767	32.008	21.117

Table 5-6. Comparison of the physical properties obtained from QM calculations and experiment.

	Lattice constant [Å]			Bulk modulus [GPa]		
	QM	Experiment	Error [%]	QM	Experiment	Error [%]
Al	4.05	4.03	0.50	75.1	79.4	5.4
Ti	2.94 c/a=1.59	2.94 c/a=1.59	0.00 0.00	113.0	110.0	2.7
Ni	3.61	3.52	2.56	197.1	187.6	5.1
Cu	3.73	3.60	3.61	132.6	142.0	6.6
Zr	3.21 c/a=1.63	3.23 c/a=1.59	0.62 2.52	91.1	97.2	6.3

Table 5-7(a). The QM results for Al-Ti.

Al [%]	Structure	E_{coh} [eV/atom]	Ω [Å^3/atom]	*B* [GPa]
0	FCC	4.79	17.580	105.7
25	$AuCu_3$	4.75	16.913	108.9
50	CsCl	4.37	16.004	109.6
	NaCl	3.87	18.523	82.4
75	$AuCu_3$	4.12	15. 629	105.5
100	FCC	3.39	16.609	75.1

Table 5-7(b). Force-field parameters for Sutton Chen force-field.

	a [Å]	*e* [meV]	*c*	*m*	*n*
Al-Ti	4.08865	0.52534	127.36737	3.23756	9.39464

Table 5-7(c). SC FF results for Al-Ti.

Al [%]	Structure	*E_ff* [eV/atom]	*E_qm* [eV/atom]	*DE* [%]	Ω_*ff* [Å^3]	Ω_*qm* [Å^3]	ΔΩ [%]
0	FCC	-4.79	-4.79	0.00	17.580	17.580	0.000
25	$AuCu_3$	-4.75	-4.75	0.00	16.955	16.913	0.248
50	CsCl	-4.47	-4.37	2.29	16.286	16.004	1.762
	NaCl	-4.13	-3.87	6.72	18.978	18.523	2.456
75	$AuCu_3$	-4.09	-4.12	0.73	16.336	15. 629	4.524
100	FCC	-3.39	-3.39	0.00	16.609	16.609	0.00

Table 5-8(a). The QM results for Al-Ni.

Al [%]	Structure	E_{coh} [eV/atom]	Ω [Å^3/atom]	*B* [GPa]
0	FCC	-4.44	11.773	197.1
25	$AuCu_3$	-4.64	12.170	176.3
50	CsCl	-4.58	12.648	153.8
	NaCl	-3.96	14.424	117.6
75	$AuCu_3$	-3.88	14.549	111.9
100	FCC	-3.39	16.609	75.1

Table 5-8(b). Force-field parameters for Sutton Chen force-field.

	a [Å]	*e* [meV]	*c*	*m*	*n*
Al-Ni	3.82434	0.42001	149.55544	4.49896	10.15049

Table 5-8(c). SC FF results for Al-Ni.

Al [%]	Structure	*E_ff* [eV/atom]	*E_qm* [eV/atom]	*DE* [%]	Ω_*ff* [Å^3]	Ω_*qm* [Å^3]	ΔΩ [%]
0	FCC	-4.44	-4.44	0.00	11.773	11.773	0.000
25	$AuCu_3$	-4.63	-4.64	0.22	11.997	12.170	1.422
50	CsCl	-4.56	-4.58	0.44	12.648	12.648	0.000
	NaCl	-4.13	-3.96	4.29	14.926	14.424	3.480
75	$AuCu_3$	-4.00	-3.88	3.09	14.418	14.549	0.900
100	FCC	-3.39	-3.39	0.00	16.609	16.609	0.000

Table 5-9(a). The QM results for Ti-Ni.

Ti [%]	Structure	E_{coh} [eV/atom]	Ω [Å^3/atom]	B [GPa]
0	FCC	-4.44	11.773	197.1
25	$AuCu_3$	-5.10	12.446	190.9
50	CsCl	-5.10	14.080	158.8
	NaCl	-4.71	15.439	130.3
75	$AuCu_3$	-4.89	15.626	125.1
100	FCC	4.79	17.580	105.7

Table 5-9(b). Force-field parameters for Sutton Chen force-field.

	a [Å]	e [meV]	c	m	n
Ti-Ni	3.86076	0.75380	93.59448	4.93429	9.66190

Table 5-8(c). SC FF results for Ti-Ni.

Ti [%]	Structure	*E_ff* [eV/atom]	*E_qm* [eV/atom]	*DE* [%]	Ω_*ff* [Å^3]	Ω_*qm* [Å^3]	ΔΩ [%]
0	FCC	-4.44	-4.44	0.00	11.773	11.773	0.000
25	$AuCu_3$	-4.91	-5.10	3.73	12.446	12.446	0.000
50	CsCl	-5.10	-5.10	0.00	13.580	14.080	3.551
	NaCl	-4.71	-4.71	0.00	15.804	15.439	2.364
75	$AuCu_3$	-4.93	-4.89	0.82	15.597	15.626	0.186
100	FCC	-4.79	-4.79	0.00	17.580	17.580	0.000

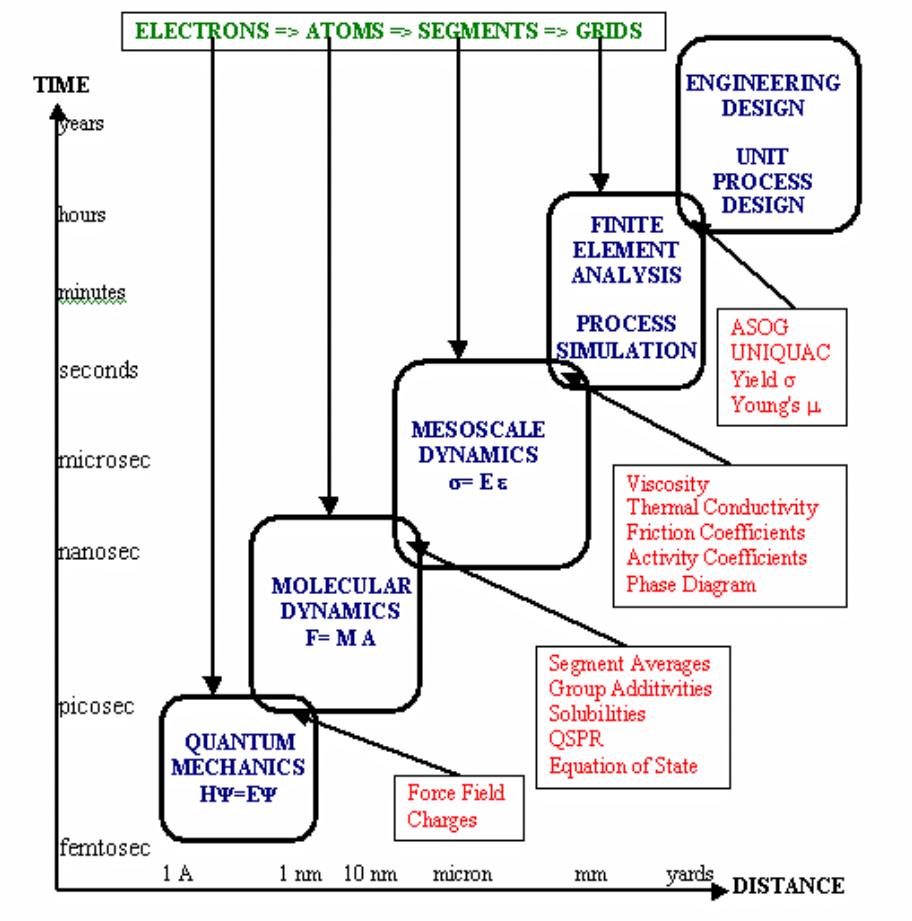

Figure 5-1. Multiscale computational hierarchy for materials simulations (Goddard, 2000).

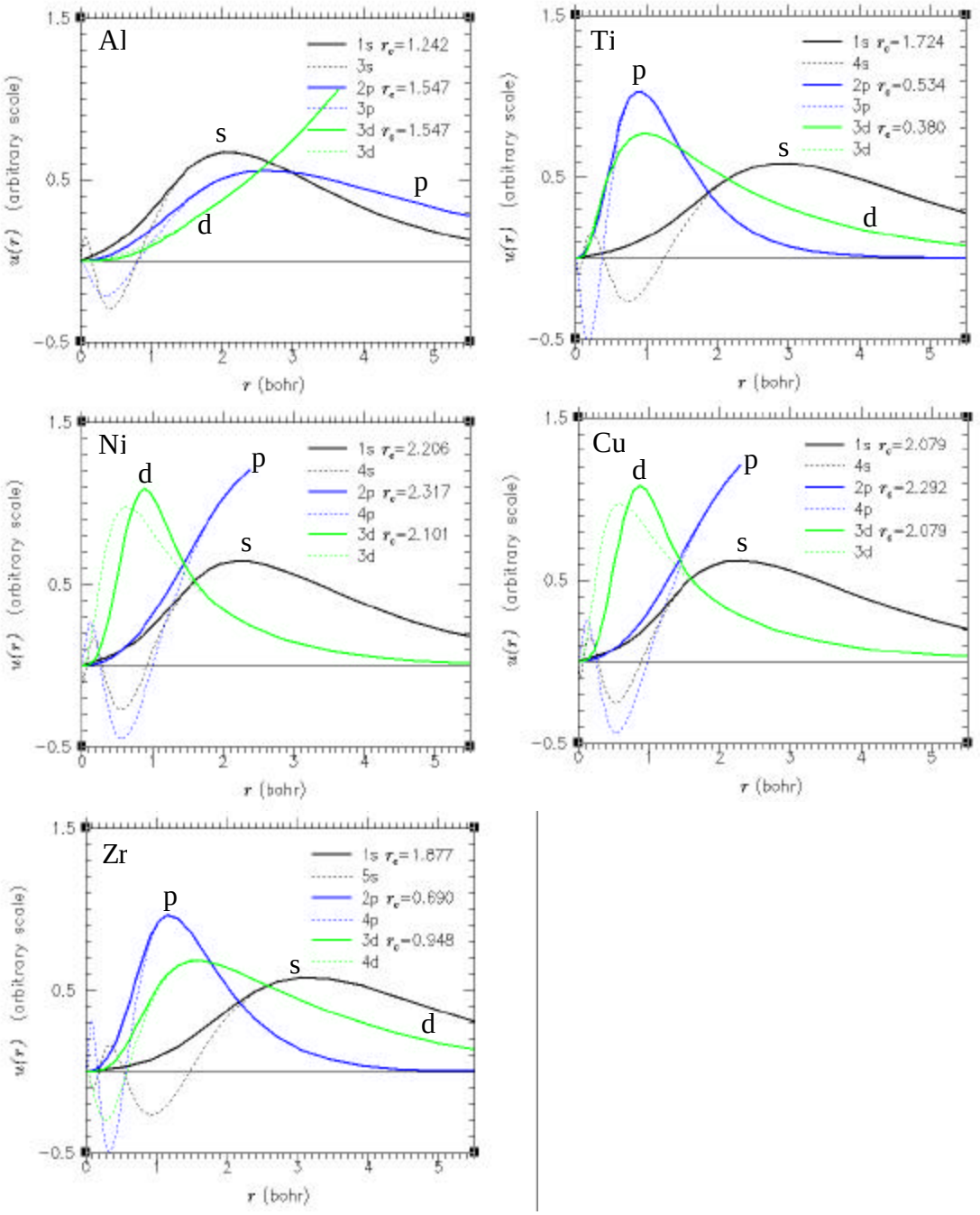

Figure 5-2. Pseudo (solid line) versus all-electron (dotted line) wave functions for Al, Ti, Ni, Cu, and Zr.

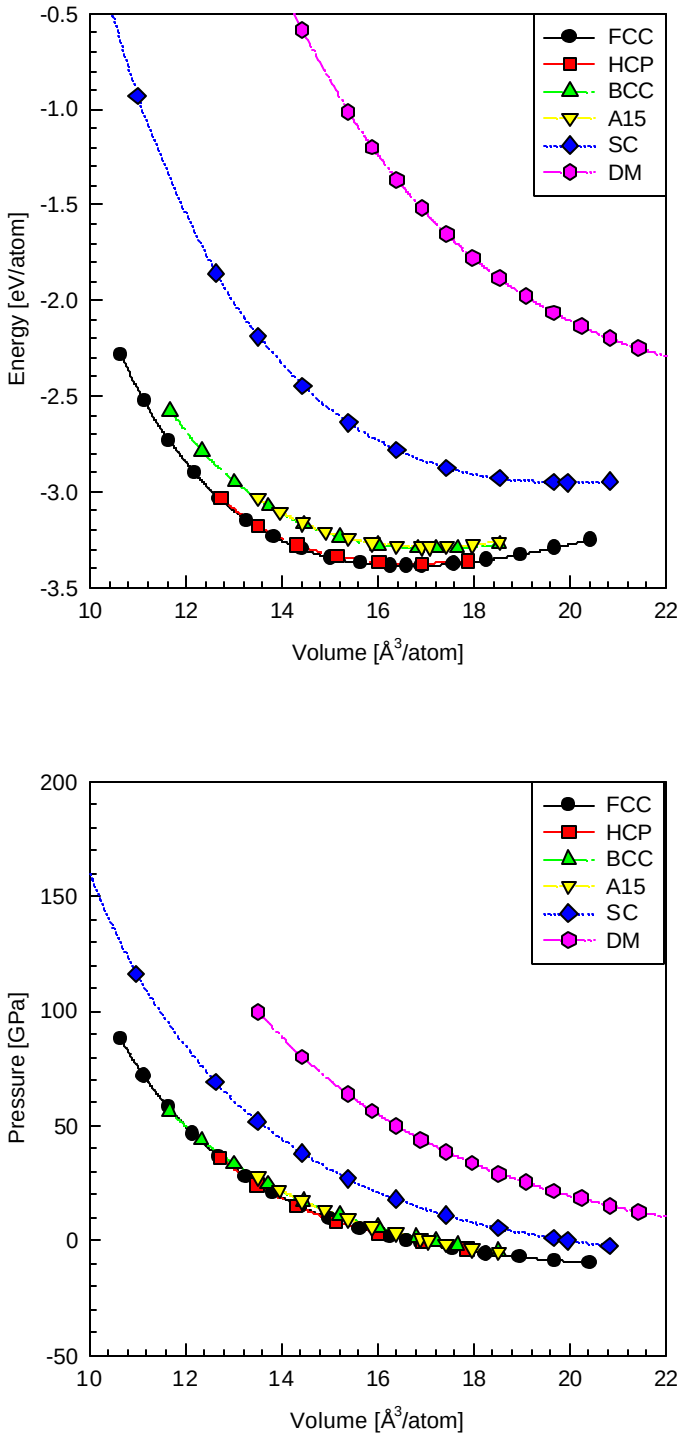

Figure 5-3. The equation of states: Al.

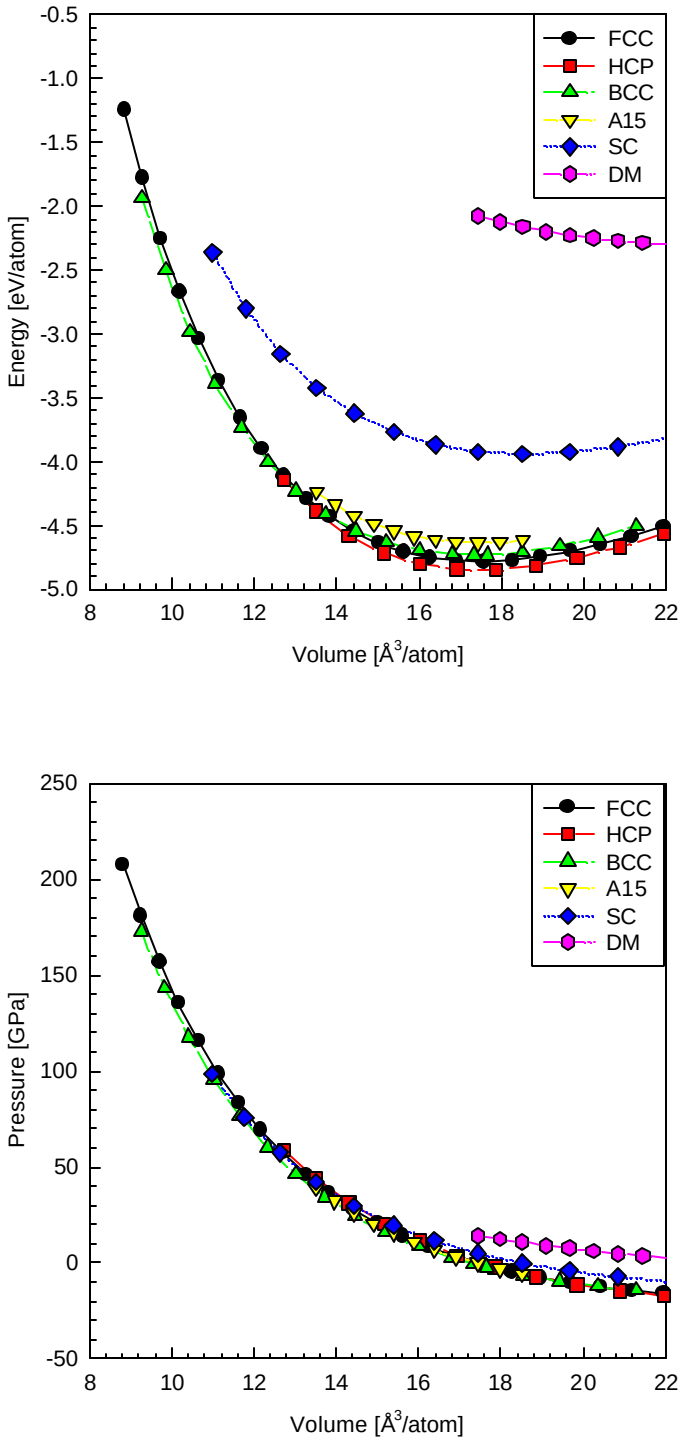

Figure 5-4. The equation of states: Ti.

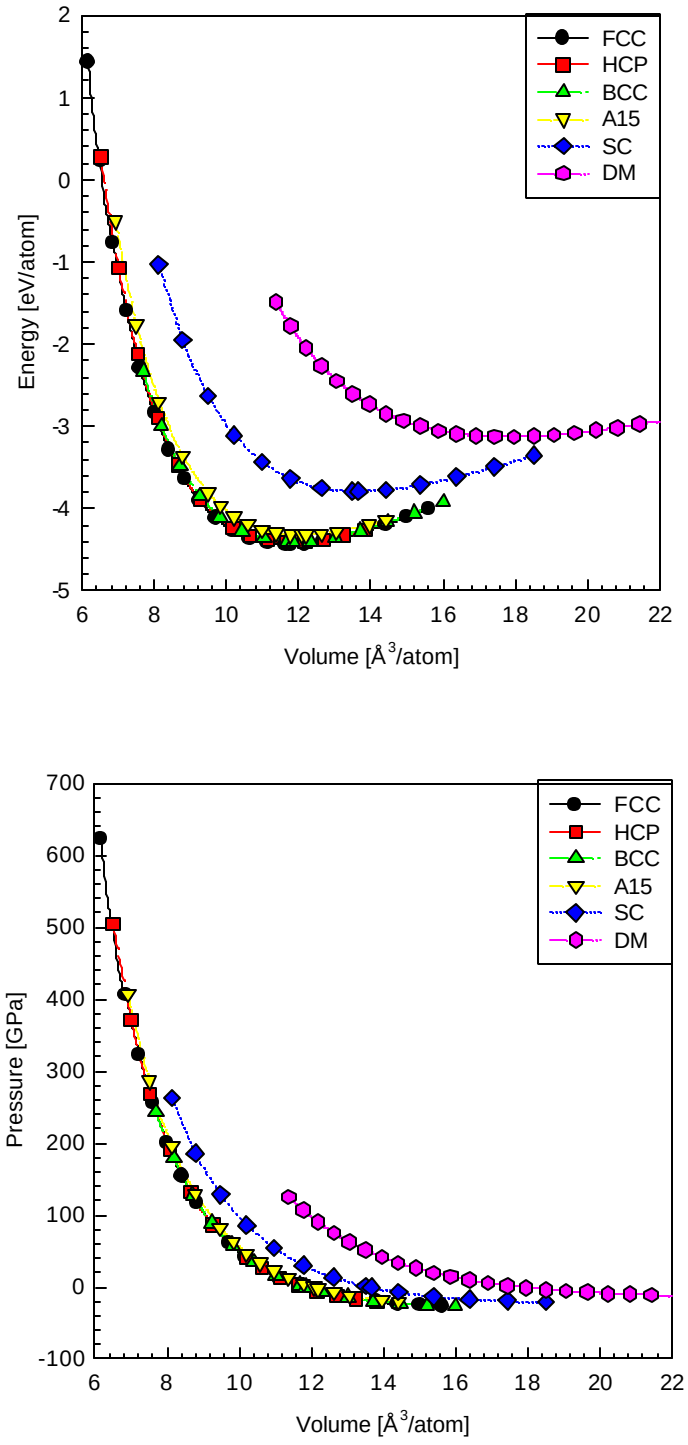

Figure 5-5. The equation of states: Ni.

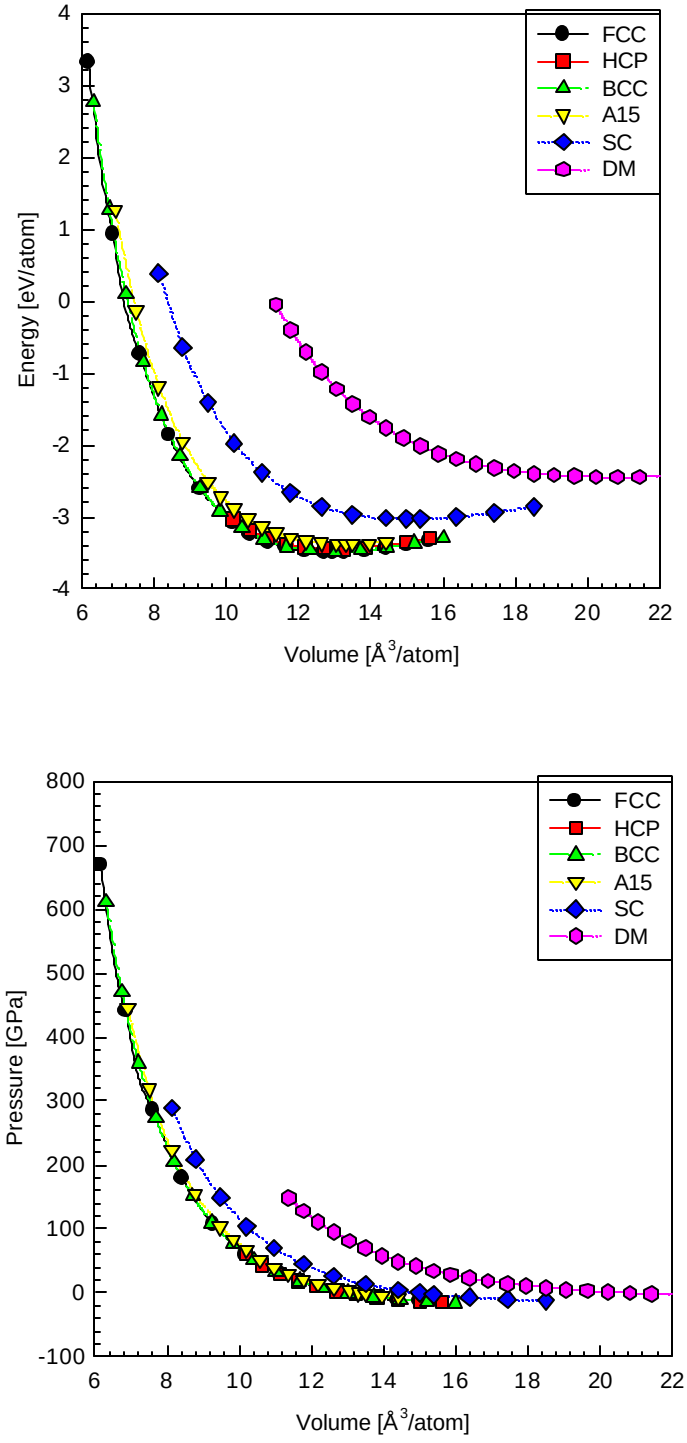

Figure 5-6. The equation of states: Cu.

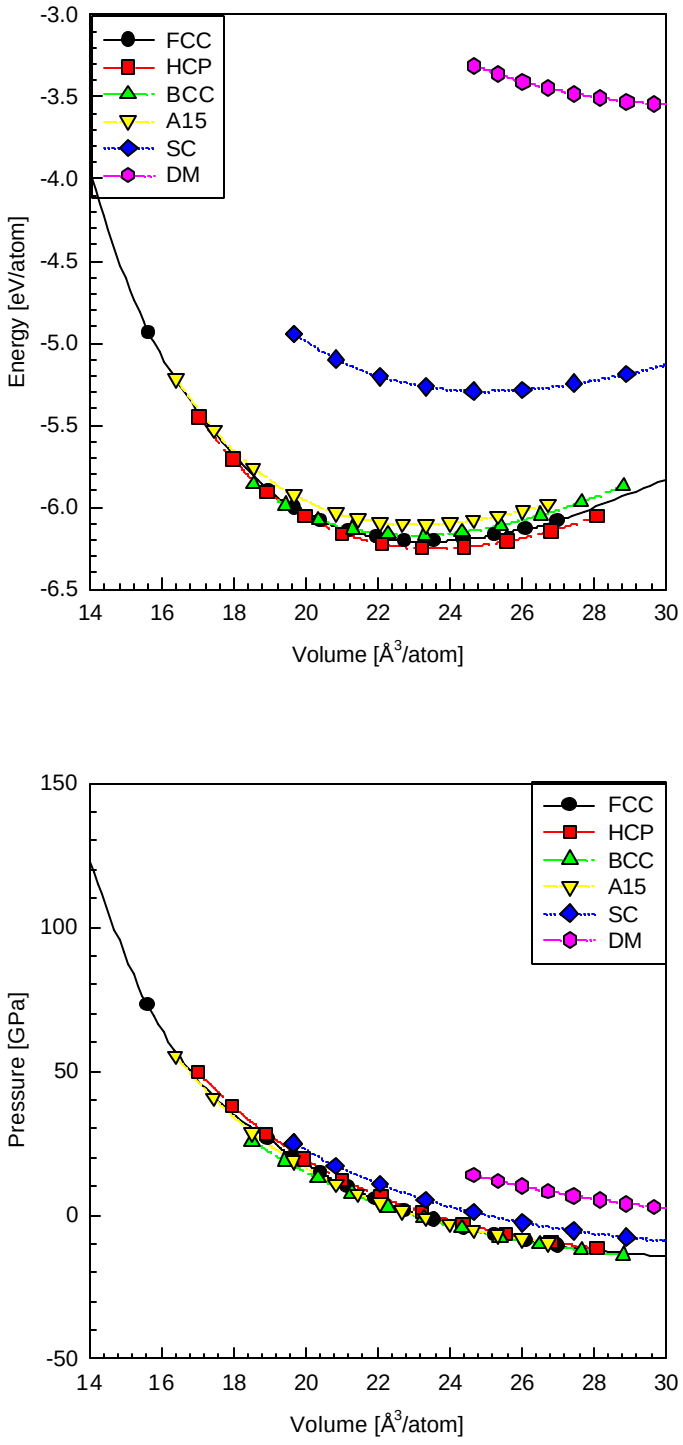

Figure 5-7. The equation of states: Zr.

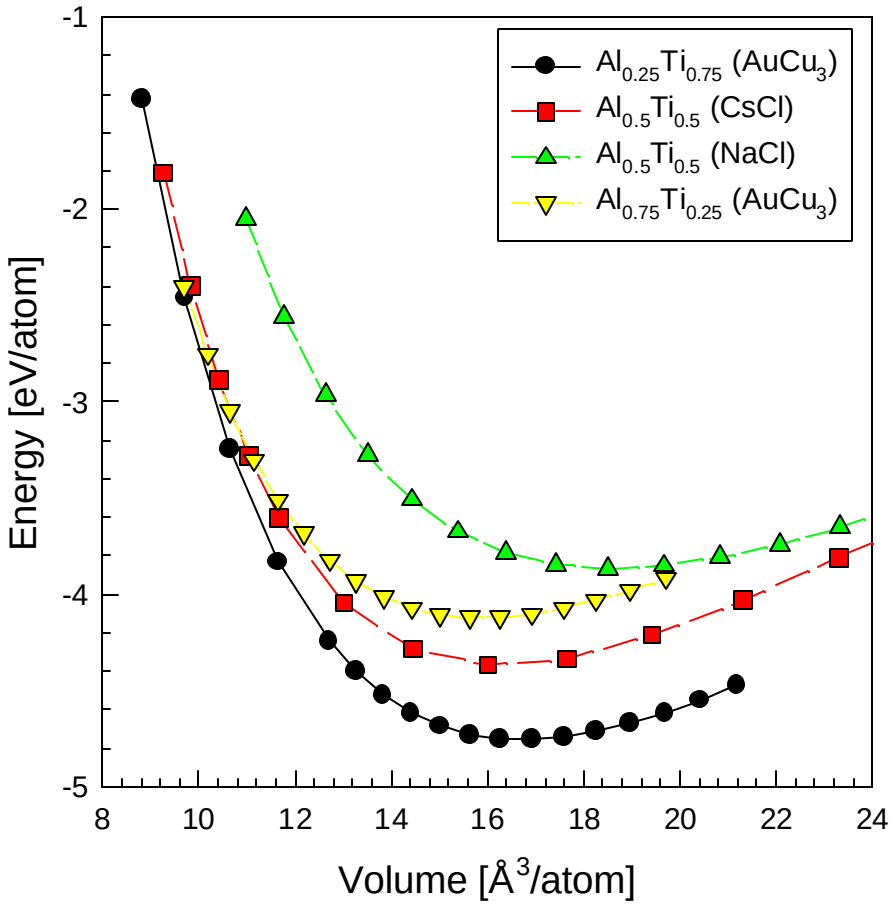

Figure 5-8. The equation of states: AlTi.

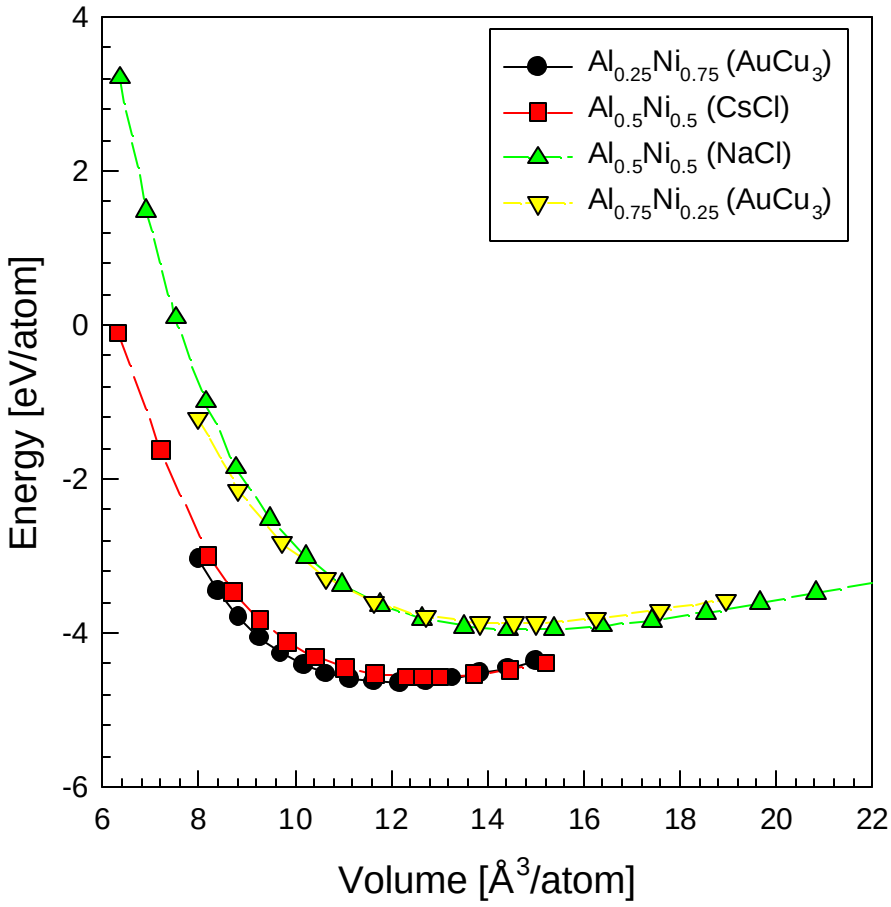

Figure 5-9. The equation of states: AlNi.

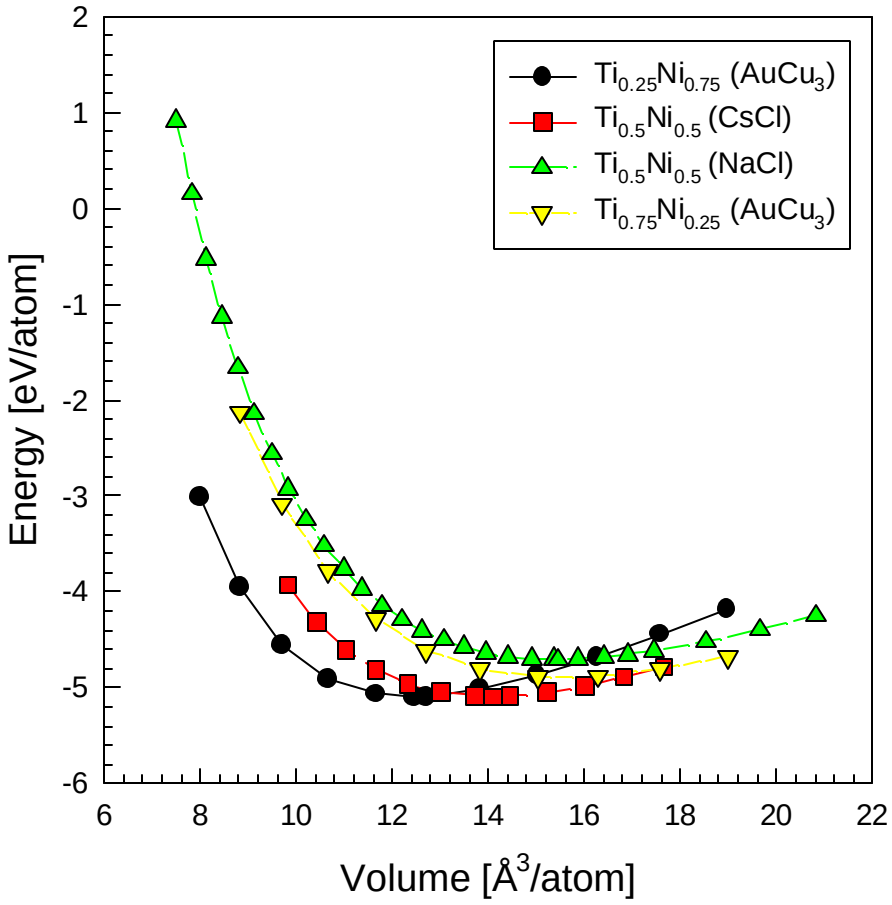

Figure 5-10. The equation of states: TiNi.

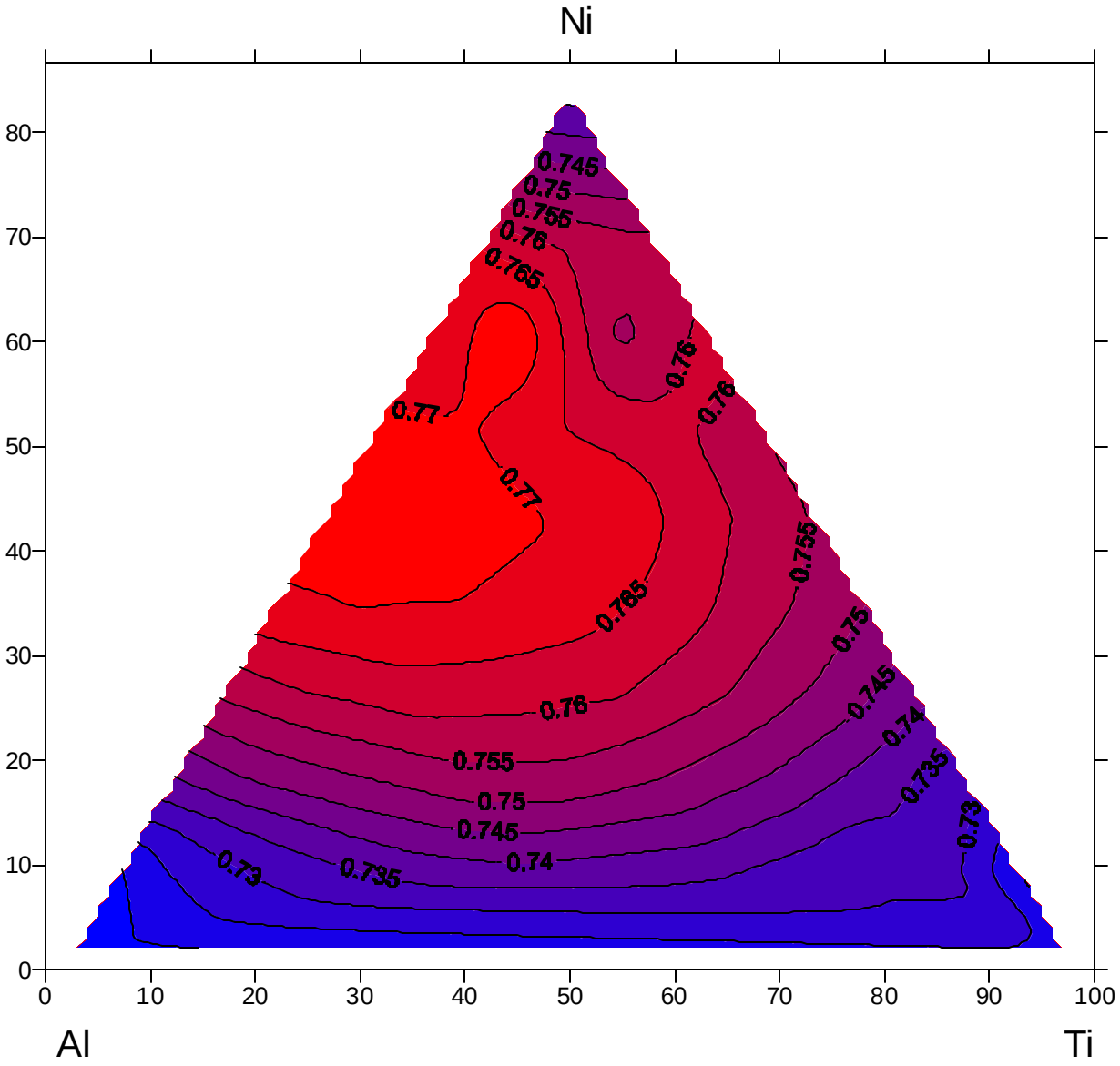

Figure 5-11. The packing fraction of AlTiNi system at T=300K.